Editors' Suggestion

Importance of one- and two-photon transitions in the strong-field dissociation of NO²⁺

Bethany Jochim [1,*] M. Zohrabi,[1] B. Gaire,[1] Tereza Uhlíková,[2] K. D. Carnes,[1] E. Wells [3] B. D. Esry,[1] and I. Ben-Itzhak[1,†]

[1]*J. R. Macdonald Laboratory, Department of Physics, Kansas State University, Manhattan, Kansas 66506, USA*
[2]*Department of Analytical Chemistry, University of Chemistry and Technology, Technická 5, 166 28 Praha 6, Czech Republic*
[3]*Department of Physics, Augustana University, Sioux Falls, South Dakota 57197, USA*

Employing a coincidence three-dimensional momentum imaging technique, we investigate the ultrafast, intense laser-induced dissociation of a metastable NO²⁺ ion beam into $N^+ + O^+$. Based on the kinetic energy release and angular distributions, measured using both 774-nm and second-order-harmonic 387-nm pulses, we show that the main processes driving dissociation in pulses of about 10^{14} W/cm² peak intensity are one- and two-photon transitions from the $X\ ^2\Sigma^+$ ground state to the $A\ ^2\Pi$ first-excited state. First-order perturbation theory calculations also corroborate these findings.

I. INTRODUCTION

Studying dynamics of molecules exposed to ultrashort laser pulses has been an ever-expanding area of research for many years now. Ultrafast photochemistry studies have made great strides in capturing detailed "snapshots" of chemical reactions [1–9]. One possible application of improved understanding of these dynamics is quantum control of molecular dynamics using ultrafast lasers [10–28]. In this application, insight into the dynamics can allow one to pinpoint the most important laser-pulse characteristics for stimulating certain molecular processes, which could in turn guide a more refined approach to control [29,30].

While ultrafast lasers are powerful tools, interpreting strong-field-driven molecular dynamics can be challenging. The multiphoton nature of the interaction along with the broad bandwidth of short pulses and the complicated electronic structure of molecules often means that several states could participate in the dynamics.

Three-dimensional (3D) momentum imaging technology [31–36], however, has proven invaluable in navigating this complexity. The rich information provided by these techniques [37–41] has been fruitfully employed to determine pathways important for dynamics [17,42–48]. For example, momentum imaging has facilitated the extensive study of the laser-induced dissociation pathways of O_2^+ [49–52]. In a more recent example, Gong *et al.* [53] reported the use of ion-electron coincidence momentum imaging of H_2 dissociative ionization to obtain pathway-resolved photoelectron angular distributions. In another example utilizing ion-electron coincidences, Kunitski *et al.* [54] reported pathway-resolved two-center interference effects in the photoelectron momentum spectra from dissociative ionization of neon dimers.

The application of 3D momentum imaging to study the strong-field dynamics of molecular-ion-beam targets [25,42,43,48,55–59] presents some particular advantages.

Ion beams allow the study of systems not available via conventional gas-phase targets. The H_3 molecule, for instance, is not stable in its ground state, while H_3^+ is [60]. Other examples include *cis-trans* acetylene [61] and vinylidene molecules [62–65], which may be produced as metastable ion beams.

Our group has also studied the laser-induced dissociation of molecular dications [66–68]. In one example [66], rapid decay of the metastable CO^{2+} molecules in flight from the ion source to the laser interaction region facilitated probing of vibrationally cold (i.e., only $v = 0$) molecules in the electronic ground state. This simplification led to different dynamics that are more tractable than the case of electronically and vibrationally hot CO^{2+} produced by the interaction of intense pulses with a neutral CO target. Therefore, ion beam studies are complementary to neutral target studies. In the present work, we will take advantage of similar simplifying traits to study NO²⁺ ions.

Also, in contrast to the case of neutral targets, for ion-beam targets, the necessity of ionization is removed. Thus, important dynamics may be driven by the lower intensity spatial "wings" of the laser pulse profile, depending on the experimental geometry. We find that in our experiment, even for high peak intensities in the low-to-mid 10^{14} W/cm² range, transitions involving low total photon numbers play a key role while ionization is practically negligible.

In this article, we report on femtosecond laser-induced dissociation of metastable NO²⁺ ions induced by a strong ($\approx 10^{14}$ W/cm²) laser pulse. We find that for the NO²⁺ beam target in this intensity regime, one- and two-photon transitions dominate. In particular, as expected, the coupling between the two lowest lying electronic states, the $X\ ^2\Sigma^+$ ground state and the $A\ ^2\Pi$ first-excited state, primarily dictates the dynamics.

II. EXPERIMENTAL TECHNIQUE

We produce an NO²⁺ ion beam by fast electron impact ionization of nitric oxide gas inside an electron-cyclotron resonance (ECR) ion source. The ions are accelerated to 9.2 keV,

---

*bjochim@phys.ksu.edu
†ibi@phys.ksu.edu

momentum analyzed using a magnet, then steered and focused by electrostatic deflectors and lenses, respectively. The cross section of the resulting collimated ion beam is about 0.9×0.9 mm^2 in the interaction region, where it intersects a beam of femtosecond laser pulses. The coincidence 3D momentum imaging method used to perform kinematically complete measurements of the ensuing dissociation has been described in earlier publications [55,69,70].

A Ti:sapphire laser system generates the linearly polarized Fourier transform-limited laser pulses at a rate of 2 kHz with a measured central wavelength of 774 nm, 2-mJ energy, and temporal duration of 27-fs FWHM (full-width at half-maximum in intensity). The bandwidth of the pulses is about 68 meV (FWHM) in energy. The pulse duration is measured using the second-order harmonic generation frequency-resolved optical gating (SHG FROG) technique [71]. Both the measured temporal and spectral intensity profiles fit nicely to Gaussian distributions. A 90-deg off-axis, $f = 203$-mm parabolic mirror focuses the laser beam onto the ion-beam target. The peak intensity [72] is controlled in the experiment by shifting the position of the focus relative to the ion-beam center along the laser propagation direction [73] while keeping the laser beam waist much smaller than the ion beam thickness [74]. We decrease the laser intensity in this manner instead of using attenuation optics, as it preserves the temporal pulse shape and increases the interaction volume, thereby improving the counting rate. We also utilize 387-nm pulses in this work, produced by sum-frequency generation in a β-barium borate (BBO) crystal [75].

III. PROPERTIES OF THE NO²⁺ BEAM

In our experiment, the NO²⁺ ions have a flight time of about 20 μs from their creation to the crossing with the laser beam. This long flight time from the ion source, along with the inherent properties of NO²⁺, simplifies our study significantly. Because the ions are formed from NO via fast vertical transitions, the Franck-Condon (FC) region of the neutral molecule is key to determining the states initially populated. Specifically, except for the $X\,^2\Sigma^+$ state, all the vibrational levels of the calculated electronic states of NO²⁺ (including all possible spin multiplets) with bound potentials in the FC region of NO have lifetimes of a few microseconds or less [76,77]. Therefore, only the $X\,^2\Sigma^+$ state is non-negligibly populated by the time the NO²⁺ molecules interact with the laser pulse.

With only the $X\,^2\Sigma^+$ state populated and taking into account that the laser field can only couple it to other doublet states, the electronic states we must consider in interpreting the dynamics are reduced to those in Fig. 1(a). Furthermore, the $v' > 12$ states of the $X\,^2\Sigma^+$ state predissociate into N⁺ + O⁺ by spin-orbit coupling with the first-excited state, $A\,^2\Pi$, within fractions of a microsecond [77] during the NO²⁺ travel to the laser crossing. Note that these N⁺ + O⁺ pairs from predissociation are readily distinguished from those formed by the laser with our momentum imaging technique. Therefore, we only probe the $X\,^2\Sigma^+$ state in vibrational levels $v' = 0$–12 in our experiment, all with lifetimes greater than 10 μs [77].

We estimate the initial population of the surviving $v' = 0$–12 vibrational levels of the $X\,^2\Sigma^+$ state by calculating FC
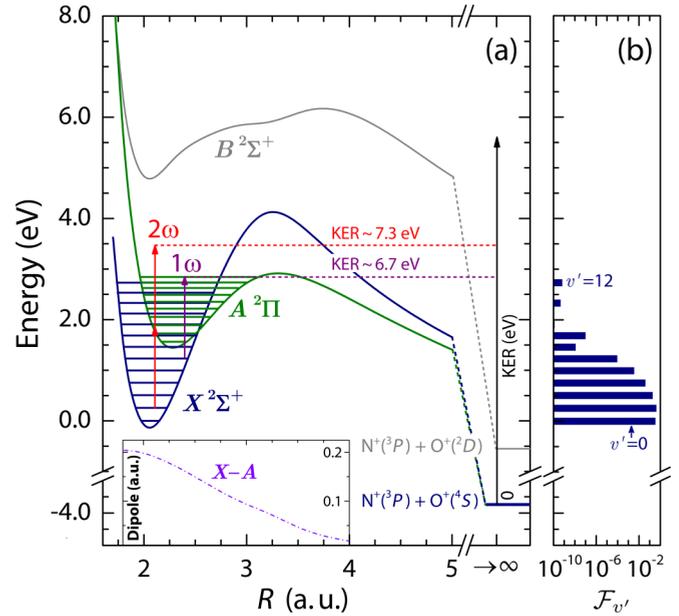
FIG. 1. (a) Lowest lying doublet potential energy curves of NO²⁺. Zero energy is defined as $v' = 0$ of the $X\,^2\Sigma^+$ state. The $B\,^2\Sigma^+$ state dissociation limit is –0.55 eV, and that of the $X\,^2\Sigma^+$ and $A\,^2\Pi$ states is –3.87 eV. These limits are from the same structure calculations [77]. The inset shows the $X\,^2\Sigma^+$–$A\,^2\Pi$ transition dipole moment [77]. (b) Franck-Condon (FC) population at the interaction point for the $X\,^2\Sigma^+$ state of NO²⁺ resulting from NO $\to$ NO²⁺ vertical ionization by fast electron impact in the ion source (see text). This distribution only includes vibrational levels that survive to the laser interaction.

factors between these states and the NO vibrational ground state. This is a reasonable approximation, as suggested by the production of H₂⁺ and its isotopologues by fast electron impact in similar ion sources [78–80]. Moreover, Refs. [79,80] also suggest that the rotational distribution of ions generated by electron impact is similar to that of the neutral molecules at room temperature [79,80]. While the populated vibrational levels of the $X\,^2\Sigma^+$ state are, rigorously speaking, resonances rather than bound states, due to their long lifetimes, we treat them as bound states in calculating the FC factors $F_{v'}$ to estimate the vibrational population [77]:

$$\mathcal{F}_{v'} = |\langle \psi_{v'} | \psi_{v=0} \rangle|^2. \tag{1}$$

Here, $\psi_{v=0}$ is the vibrational ground state wave function of NO, and $\psi_{v'}$ is the wave function of vibrational state v' in the $X\,^2\Sigma^+$ ground state of NO²⁺. The vibrational wave functions were calculated using a phase-amplitude method [81], assuming $J = 0$. The resulting FC factors are shown in Fig. 1(b). Note that most of the initial population is in the $v' = 0$–5 states.

IV. RESULTS AND DISCUSSION

Our measurements presented here are performed with laser intensities in the low to mid-10¹⁴ W/cm² range at near-infrared wavelengths, for which one may expect ionization to be significant based on studies of ionization of neutral molecules. See, for example, the single and double ionization
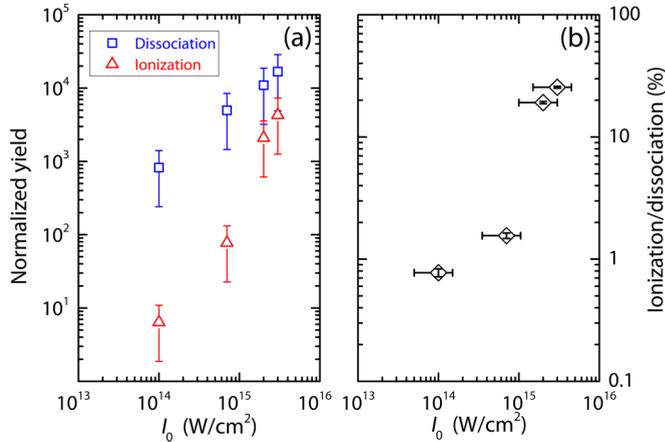
FIG. 2. The ionization and dissociation rates of NO^{2+} by a 27-fs, 774-nm pulse as a function of peak intensity I_0. (a) The yields of dissociation ($N^+ + O^+$) and ionization ($N^{2+} + O^+$ and $N^+ + O^{2+}$) normalized to the same focal volume as the highest intensity, assuming stable beam current, laser pulses, and beam crossing throughout these consecutive measurements. The main sources of errors are instabilities in these quantities. (b) The ionization-to-dissociation ratio. Note that ionization is of the order of 1% or less for intensities below 5×10^{14} W/cm^2.

FIG. 3. [(a), (b)] The yield of $N^+ + O^+$ as a function of KER and $\cos\theta$ for 774-nm pulses with peak intensities 4×10^{14} and 1×10^{14} W/cm^2, respectively. Recall that θ is the angle between the N^+ momentum and the laser polarization. [(c), (d)] 1D KER projections of panels (a) and (b), respectively. In panel (c), the purple and red combs indicate expected KER values for one- and two-photon $X\,^2\Sigma^+ \rightarrow A\,^2\Pi$ transitions, respectively. The numbers above the combs indicate the initial vibrational level v' of the $X\,^2\Sigma^+$ state for these transitions.

rates measured by Cornaggia and Hering for a few molecules [82]. Similarly, ionization of molecular ions like H_2^+ [55,83] and D_3^+ [83–85] is non-negligible in this intensity range. Ionization of NO^{2+} and dications in general requires the removal of a third electron, and therefore, we expect it to be like double ionization of D_3^+, which has an appearance intensity in the low to mid-10^{15} W/cm^2 range [60,85].

To verify this expectation, we measured the ionization rate of NO^{2+} (normalized to a fixed focal volume) and the ratio of ionization to dissociation, both shown in Fig. 2 as a function of laser intensity. It can be clearly seen that ionization is about 1% of dissociation or less at the intensities we focus on here. In addition to the impact of the large ionization potential to overcome for removing the third electron, the ionization to dissociation ratio is also suppressed by two additional factors. First, intensity averaging over the focal volume favors contributions from lower intensities found in the "wings" of the laser focus in the radial direction because of their larger volume in our experimental geometry [73,86]. Second, the relevant potential energy curves (see Fig. 1) are very steep beyond $R \approx 4$ a.u. due to the Coulomb repulsion between the charge fragments, leading to rapid dissociation. Given that one or two photons can initiate dissociation, as we show below, dissociation of NO^{2+} in the focus is likely to occur on the laser pulse's leading edge. Before the laser intensity peaks, the resulting rapid dissociation may stretch the molecule well beyond the internuclear distance where ionization is enhanced, therefore suppressing ionization [83,87]. Having established that NO^{2+} dissociation dominates in the present intensity regime, we explore these processes in further detail.

Informed by previous studies of H_2^+ and other diatomic molecules [50], we expect that, given the energy separation of the $X\,^2\Sigma^+$ and $A\,^2\Pi$ states relative to the photon energy, illustrated in Fig. 1(a), these states would be easily coupled by

the absorption of one or two 774-nm (about 1.60-eV energy) photons. The next-lowest doublet state, $B\,^2\Sigma^+$, is well separated from these lowest two states. Thus, at laser intensities at which four-photon transitions (such as would be required for $N^+ + O^+$ dissociation on the $B\,^2\Sigma^+$ state starting from $v' = 1$) are negligible, one would expect transitions between the $X\,^2\Sigma^+$ and $A\,^2\Pi$ states involving fewer than four photons to be the most important.

We focus on dissociation of NO^{2+} into $N^+ + O^+$, measured in coincidence. From these measurements, we extract the kinetic energy release (KER) and angular distributions for the laser-induced dissociation. Density plots of the measured $N^+ + O^+$ yield as a function of KER and $\cos\theta$ as well as KER projections are shown in Fig. 3 for 1×10^{14} and 4×10^{14} W/cm^2 peak laser intensities. Note that θ is defined as the angle between the momentum of the N^+ fragment and the laser polarization.

As shown by this figure, in this intensity regime, $N^+ + O^+$ breakup is more likely perpendicular to the laser polarization direction. Moreover, the KER spectrum has two peaks centered at about 6.5 and 7.5 eV, as clearly seen in Figs. 3(c) and 3(d). We will argue below that these peaks are due to one- and two-photon (total) $X\,^2\Sigma^+ \rightarrow A\,^2\Pi$ transitions, respectively.

A. One-photon transitions

In interpreting our measurements, we are guided by the "standard" approach to determine plausible strong-field dissociation pathways by examining the KER and angular distributions (see, for example, Ref. [50]). The following

TABLE I. Calculated tunneling lifetimes [77] and corresponding energy widths for $A\,^2\Pi$ state vibrational resonances v''.

v''	$\tau_{v''}\,(\mu s)$	Energy width (eV)
5	6.78×10^{12}	1×10^{-22}
6	3.45×10^{7}	2×10^{-15}
7	6.44×10^{2}	1×10^{-12}
8	4.48×10^{-2}	1×10^{-8}
9	1.42×10^{-5}	5×10^{-5}

discussion will assume that $J = 0$. While higher J states could be involved, the small resulting shifts in energy would not change our general conclusions. Finally, we will validate the proposed pathways with first-order perturbation theory.

1. Kinetic energy release

Let us consider the lower energy peak centered at around 6.5 eV in Figs. 3(c) and 3(d). The purple comb above the KER distribution indicates the expected KER values for one-photon $X\,^2\Sigma^+ \to A\,^2\Pi$ transitions from the indicated initial vibrational levels v' of the $X\,^2\Sigma^+$ state and leading to $N^+ + O^+$ dissociation. One can see that such transitions starting from $v' = 3$, 4, and 5 match the measured KER for the 6.5-eV peak reasonably well. First, a one-photon near-resonant transition from $v' = 3$ results in population of $v'' = 5$ of the $A\,^2\Pi$ state, which has a lifetime too long for $N^+ + O^+$ to be detected. Further, all resonances with $v'' \leqslant 7$ cannot contribute because they have long tunneling lifetimes and are dominated by radiative decay, which produces nondissociative states. For reference, some tunneling lifetimes of the $A\,^2\Pi$ state resonances are listed in Table I.

Transitions starting from $v' = 4$ and 5, on the other hand, can result in population of the $A\,^2\Pi$ vibrational resonances $v'' = 8$ and 9. The short tunneling lifetimes of $v'' = 8$ and 9 allow $N^+ + O^+$ to be detected.

2. Angular distributions

Next, we shift our attention to the angular distribution of the lower KER peak. Assuming that the initial angular distribution of the NO^{2+} molecules is isotropic, the change of the angular momentum quantum number, $\Delta\Lambda$, for the transition imprints itself on the angular distribution. Specifically, for n parallel ($\Delta\Lambda = 0$) transitions, the expected angular distribution follows $\cos^{2n}\theta$. For n perpendicular ($\Delta\Lambda = \pm 1$) transitions, on the other hand, the expected distribution is $\sin^{2n}\theta$ [49,50]. Strictly speaking, these angular distributions are expected for $J = 0$, though they have been used commonly in studies where the angular momentum distribution extended to somewhat higher values of J. In a previous study [66], we have shown that the measured angular distribution upon dissociation of CO^{2+} initially in $J = 1$ matches a $\sin^2\theta$ distribution. Our theory, however, showed clearly that the $\sin^2\theta$ distribution is only approximate, and the nonisotropic distribution is due to the angular distributions associated with the magnetic quantum numbers, M_J. We expect a similar trend for somewhat higher J values, but establishing the accuracy of this approximation is beyond the scope of this work.
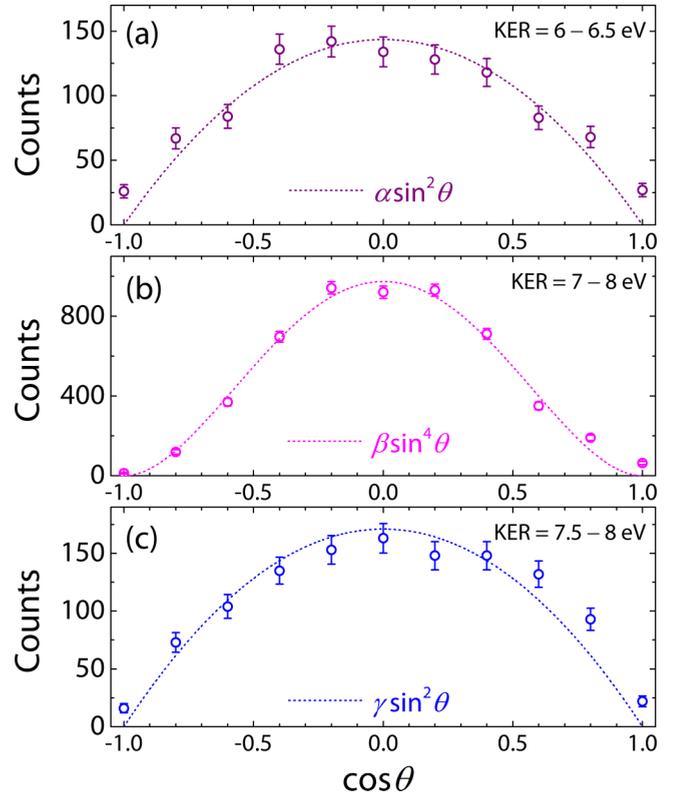
FIG. 4. Measured angular distributions of narrow KER ranges (indicated on each panel) for (a) 774 nm, $1 \times 10^{14}\,\text{W/cm}^2$, (b) 774 nm, $4 \times 10^{14}\,\text{W/cm}^2$, and (c) 387 nm, $1 \times 10^{14}\,\text{W/cm}^2$. The data in each panel are fitted with the indicated angular distribution (see text).

The angular distribution for the 6.5-eV feature, shown in Fig. 4(a), fits a $\sin^2\theta$ distribution reasonably well, further supporting the idea that a one-photon $X\,^2\Sigma^+ \to A\,^2\Pi$ transition is responsible for the observed dissociation. Note that this $\sin^2\theta$ function does not match the data near $\cos\theta = \pm 1$ in Fig. 4(a), suggesting a minor contribution of another process involving parallel transitions.

3. Perturbation theory

As the KER and angular distributions suggest the dominant contributions of one-photon processes, we apply first-order perturbation theory to confirm the dissociation pathways leading to the lower KER peak.

The transition probabilities given by first-order perturbation theory in the rotating-wave approximation [84] are (in atomic units)

$$\frac{dP_{v'}}{dE} \propto |D_{v'}(E)|^2 \exp\left[-\left(\frac{2\sqrt{\ln 2}(\omega - \omega_{fi})}{\Delta\omega}\right)^2\right]. \quad (2)$$

Here, $\Delta\omega$ is the laser bandwidth (FWHM). The quantity ω_{fi} is given by $E - E_{v'}$, where E is the final total energy and $E_{v'}$ is the energy of the initial vibrational level in the $X\,^2\Sigma^+$ state. The final total energy is related to the KER as follows:

$$\text{KER} = E - E_\infty, \quad (3)$$

where E_∞ is the dissociation limit. The dipole matrix element is given by

$$D_{v'}(E) = \langle \psi_E | D | \psi_{v'} \rangle. \quad (4)$$

Here, $\psi_E(R)$ is an energy-normalized vibrational resonance wave function below the barrier or continuum wave function above the barrier in the $A\ ^2\Pi$ state. The $X\ ^2\Sigma^+ - A\ ^2\Pi$ transition dipole moment, shown in the inset of Fig. 1(a), is denoted as D.

To compute the KER distribution, the transition probabilities in Eq. (2) are weighted by the estimated initial vibrational population in Eq. (1). Thus, the KER distribution for a given initial vibrational level v' is

$$N(\text{KER})_{v'} = \mathcal{F}_{v'} \frac{dP_{v'}}{dE}. \quad (5)$$

In addition, regarding dissociation due to the decay of populated $A\ ^2\Pi$ state vibrational resonances, one must account for the influence of tunneling lifetimes. Specifically, do the dissociating vibrational resonances decay completely and does dissociation in flight [88] affect our observation? These questions must be examined for each particular target molecule and set of experimental conditions. For the present case, the $A\ ^2\Pi$ state resonances that contribute non-negligibly to dissociation ($v'' = 8$ and $v'' = 9$) decay completely and are observed as prompt $N^+ + O^+$ breakup. The lower vibrational states have lifetimes too long to allow dissociation in our experiment.

The computed KER distributions for the highest probability peaks are shown in Fig. 5(a). The peaks of other transitions, such as $v' = 3 \rightarrow v'' = 8$, are too small to be visible in the figure. The sharp peaks for dissociation via transitions from $X\ ^2\Sigma^+$ ($v' = 4$ and 5) to the $A\ ^2\Pi$ ($v'' = 8$ and 9) resonances arise due to the narrow widths of those resonances [77] (see Table I). Dissociation via these transitions should dominate, as shown by Fig. 5(a). For comparison, the area under the $v' = 5 \rightarrow v'' = 9$ peak is more than three orders of magnitude larger than the $v' = 7 \rightarrow A\ ^2\Pi$ vibrational continuum peak. The initial vibrational population decreases with increasing v', as shown in Fig. 1(b), decreasing the contribution of the "bound" free transitions.

The calculated KER peaks are also convoluted with the estimated KER resolution, treated as a Gaussian distribution with width of 0.49 eV (FWHM) at 6.5-eV KER [89]. The convoluted distributions were added together and scaled to the experimental data at the lower KER peak. The result, shown in Fig. 5(b) by the navy dash-dotted curve, agrees reasonably well with the data, but with a small shift to higher KER. This observed energy shift could be due to an energy scaling uncertainty of about 3% in our imaging setup [84].

Finally, it is important to note that while the lower KER peak is reasonably well reproduced by our perturbation theory calculations, the higher KER peak is not. Thus, one-photon dissociation is not likely to be the dominant contribution to this higher energy peak.
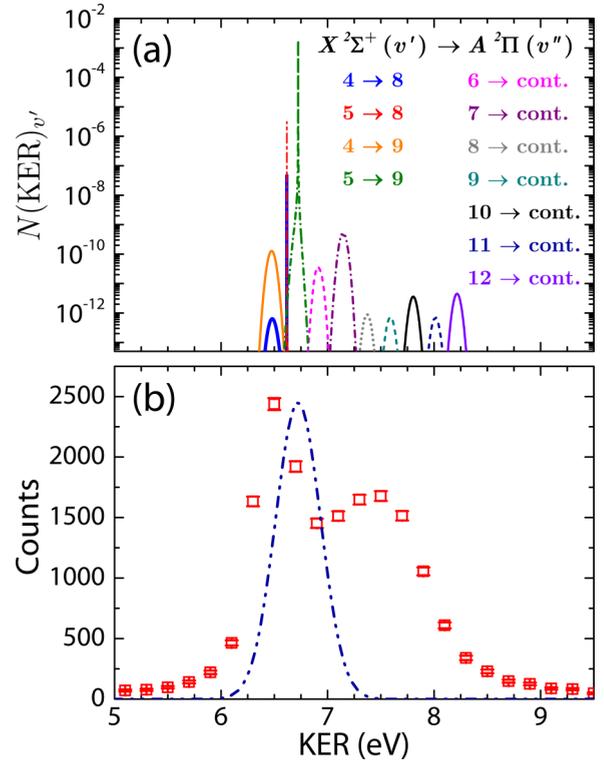
FIG. 5. (a) The KER spectra computed using first-order perturbation theory. Here, "cont." indicates transitions to the vibrational continuum of the $A\ ^2\Pi$ state. Note that there are two sharp peaks due to resonances at around 6.6-eV KER, one for $v' = 4 \rightarrow v'' = 8$ (blue, which also includes a weaker and broader feature at lower energy) and another for $v' = 5 \rightarrow v'' = 8$ (red). (b) Comparison of the computed and experimental KER spectra for 774-nm and peak intensity of $4 \times 10^{14}\ \text{W/cm}^2$. The navy blue dash-dotted curve shows the calculated dissociation probability convoluted with the experimental resolution (see text), summed over all transitions, and scaled to match the measured peak at around 6.5 eV.

B. Two-photon transitions

1. Kinetic energy release

Shown by the purple comb in Fig. 3(c), one-photon transitions from higher vibrational states of the $X\ ^2\Sigma^+$ ground state, for example $v' = 7$–9, would lead to KER matching that of the 7.5-eV peak. As mentioned above, however, these vibrational states have low initial population. Also, transitions from them to the $A\ ^2\Pi$ vibrational continuum are likely to only contribute a small fraction to the 7.5-eV KER feature, according to our first-order perturbation theory calculations. On the other hand, two-photon transitions from lower vibrational levels of the $X\ ^2\Sigma^+$ state, such as $v' = 0$–2, which have higher initial population, lead to KER matching the higher energy peak. These transitions are illustrated in Fig. 1(a) by the red "2ω" arrows, and their expected KER values are indicated by the red comb in Fig. 3(c).

Among the possible two-photon pathways leading to $N^+ + O^+$ dissociation are those involving intermediate near-resonant steps, in addition to $X\ ^2\Sigma^+ \rightarrow A\ ^2\Pi$ transitions due to the nonresonant absorption of two photons. For example, one photon may be absorbed to drive a near-resonant
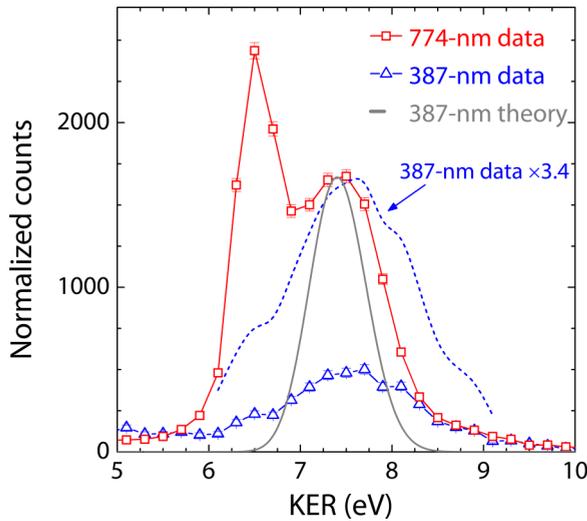
FIG. 6. The KER spectra for 774-nm (peak intensity 4×10^{14} W/cm^2) and 387-nm (peak intensity 1×10^{14} W/cm^2) central wavelength pulses. The dashed blue line corresponds to the 387-nm results scaled to match the amplitude of the higher KER peak in the 774-nm spectrum. The gray line represents the first-order perturbation theory result at 387 nm, convoluted with the KER resolution and scaled to the 774-nm data.

$X\ ^2\Sigma^+\ (v' = 1) \rightarrow A\ ^2\Pi\ (v'' = 2)$ transition, followed by the absorption of a second photon to drive a near-resonant $A\ ^2\Pi\ (v'' = 2) \rightarrow X\ ^2\Sigma^+\ (v' = 16)$ transition. The $v' = 16$ vibrational resonance of the $X\ ^2\Sigma^+$ state decays rapidly via spin-orbit coupling [77] leading to $N^+ + O^+$ dissociation.

2. Angular distributions

The angular distribution of the second KER peak, shown in Fig. 4(b), matches well with a $\sin^4\theta$ distribution, i.e., the expected distribution for two perpendicular transitions, such as the $X\ ^2\Sigma^+ \rightarrow A\ ^2\Pi \rightarrow X\ ^2\Sigma^+$ process suggested above. The angular distribution thus further supports the dominant role of two-photon transitions for the higher KER peak. This measured distribution does not, however, allow definitive exclusion of a small contribution from one-photon perpendicular transitions, i.e., $\sin^2\theta$.

3. Verifying with second-order harmonic

To further confirm the role of two-photon transitions at 774 nm, we performed an additional measurement employing second-order harmonic pulses at about 387-nm central wavelength. The pulses have a temporal duration of about 50 fs (FWHM in intensity) and bandwidth of about 5 nm (FWHM). As a simple matter of energy conservation, it is expected that the one-photon peak for the 387-nm pulses would appear at the same KER as the two-photon peak for the 774-nm pulses.

The 387-nm KER spectrum does indeed match up reasonably well with the higher KER peak measured with 774-nm pulses, shown in Fig. 6. Furthermore, the angular distribution for the peak in the 387-nm data in Fig. 4(c) agrees well with a $\sin^2\theta$ distribution, confirming that it is due to the expected $X\ ^2\Sigma^+ \rightarrow A\ ^2\Pi$ one-photon perpendicular transitions. Finally, the $X\ ^2\Sigma^+ \rightarrow A\ ^2\Pi$ KER spectrum calculated

in first-order perturbation theory for 387-nm photons, shown in Fig. 6, agrees reasonably well with the 387-nm data. These calculations are for transitions from initial vibrational states $v' = 0$–12 to the $A\ ^2\Pi$ state vibrational continuum. Moreover, these results are convoluted with the estimated instrumental resolution as before.

As one may note from Fig. 6, first-order perturbation theory results in a peak that is noticeably narrower than that in the 387-nm measurement. The broadening of the measured spectrum relative to the theory is likely due to some leakage of the 774-nm fundamental beam through the dichroic filter used in our second-order harmonic generation setup. We estimate this leakage to be on the order of 1%. Under these circumstances, the low-energy edge of the KER spectrum could be due to the one-photon 774-nm transitions discussed in Sec. IV A. The high-energy portion of the KER spectrum, on the other hand, could be due to two-photon transitions involving absorption of one photon of the fundamental beam followed by absorption of one photon of the second-order harmonic beam. While the angular distributions could in theory provide an indication of these pathways, the limited statistics of our 387-nm data prevent this. As the calculations reproduce the main feature in the data, further exploration is beyond the scope of this discussion.

V. SUMMARY AND CONCLUSIONS

In strong-field studies of NO^{2+} fragmentation starting from neutral NO targets [90–93], the absorption of more than twenty 800-nm photons is required for double ionization. Hence, the NO^{2+} molecules probed in these experiments are most likely born near the laser beam focus and near the peak of the temporal profile. In contrast, in our study of an NO^{2+} ion beam, since ionization is not needed, one can expect low-order processes occurring in lower-intensity regions of the laser focal volume to play a more significant role. The influence of intensity averaging in our measurements is also augmented by the experimental geometry in which the ion beam width is much greater than the laser spot size. At the peak laser intensity of about 10^{14} W/cm^2, highlighted in this paper, ionization of NO^{2+} constitutes less than 1% of dissociation.

Indeed, as we have shown, the dominant dissociation pathways at these intensities are one- and two-photon transitions involving the lowest two electronic states, $X\ ^2\Sigma^+$ and $A\ ^2\Pi$. Through the examination of the KER and angular distributions at 774- and 387-nm central wavelength along with first-order perturbation theory calculations, we have uncovered the most likely pathways leading to the observed dissociation.

[1] A. H. Zewail, Angew. Chem., Int. Ed. **39**, 2586 (2000).

[2] A. S. Alnaser, I. Litvinyuk, T. Osipov, B. Ulrich, A. Landers, E. Wells, C. M. Maharjan, P. Ranitovic, I. Bochareva, D. Ray, and C. L. Cocke, J. Phys. B **39**, S485 (2006).

[3] S. De, I. A. Bocharova, M. Magrakvelidze, D. Ray, W. Cao, B. Bergues, U. Thumm, M. F. Kling, I. V. Litvinyuk, and C. L. Cocke, Phys. Rev. A **82**, 013408 (2010).

[4] M. A. Yandell, S. B. King, and D. M. Neumark, J. Am. Chem. Soc. **135**, 2128 (2013).

[5] R. D. Levine, Proc. Natl. Acad. Sci. USA **114**, 13594 (2017).

[6] M. S. Schuurman and A. Stolow, Annu. Rev. Phys. Chem. **69**, 427 (2018).

[7] J. Yang, X. Zhu, T. J. A. Wolf, Z. Li, J. P. F. Nunes, R. Coffee, J. P. Cryan, M. Gühr, K. Hegazy, T. F. Heinz, K. Jobe, R. Li, X. Shen, T. Veccione, S. Weathersby, K. J. Wilkin, C. Yoneda, Q. Zheng, T. J. Martinez, M. Centurion *et al.*, Science **361**, 64 (2018).

[8] T. Ando, A. Shimamoto, S. Miura, A. Iwasaki, K. Nakai, and K. Yamanouchi, Commun. Chem. **1**, 7 (2018).

[9] Y. Malakar, W. L. Pearson, M. Zohrabi, B. Kaderiya, Kanaka Raju P., F. Ziaee, S. Xue, A. T. Le, I. Ben-Itzhak, D. Rolles, and A. Rudenko, Phys. Chem. Chem. Phys. **21**, 14090 (2019).

[10] P. Brumer and M. Shapiro, Annu. Rev. Phys. Chem. **43**, 257 (1992).

[11] A. H. Zewail, Pure Appl. Chem. **72**, 2219 (2000).

[12] M. Shapiro and P. Brumer, Rep. Prog. Phys. **66**, 859 (2003).

[13] M. Dantus and V. V. Lozovoy, Chem. Rev. **104**, 1813 (2004).

[14] A. S. Alnaser, X. M. Tong, T. Osipov, S. Voss, C. M. Maharjan, P. Ranitovic, B. Ulrich, B. Shan, Z. Chang, C. D. Lin, and C. L. Cocke, Phys. Rev. Lett. **93**, 183202 (2004).

[15] D. Cardoza, B. J. Pearson, M. Baertschy, and T. Weinacht, J. Photochem. Photobiol. A **180**, 277 (2006).

[16] P. Nuernberger, G. Vogt, T. Brixner, and G. Gerber, Phys. Chem. Chem. Phys. **9**, 2470 (2007).

[17] J. McKenna, A. M. Sayler, F. Anis, B. Gaire, N. G. Johnson, E. Parke, J. J. Hua, H. Mashiko, C. M. Nakamura, E. Moon, Z. Chang, K. D. Carnes, B. D. Esry, and I. Ben-Itzhak, Phys. Rev. Lett. **100**, 133001 (2008).

[18] E. Wells, J. McKenna, A. M. Sayler, B. Jochim, N. Gregerson, R. Averin, M. Zohrabi, K. D. Carnes, and I. Ben-Itzhak, J. Phys. B: At., Mol. Opt. Phys. **43**, 015101 (2009).

[19] D. Geißler, P. Marquetand, J. González-Vázquez, L. González, T. Rozgonyi, and T. Weinacht, J. Phys. Chem. A **116**, 11434 (2012).

[20] E. Wells, C. E. Rallis, M. Zohrabi, R. Siemering, B. Jochim, P. R. Andrews, U. Ablikim, B. Gaire, S. De, K. D. Carnes, B. Bergues, R. de Vivie-Riedle, M. F. Kling, and I. Ben-Itzhak, Nat. Commun. **4**, 2895 (2013).

[21] T. Rathje, A. M. Sayler, S. Zeng, P. Wustelt, H. Figger, B. D. Esry, and G. G. Paulus, Phys. Rev. Lett. **111**, 093002 (2013).

[22] N. G. Kling, K. J. Betsch, M. Zohrabi, S. Zeng, F. Anis, U. Ablikim, B. Jochim, Z. Wang, M. Kübel, M. F. Kling, K. D. Carnes, B. D. Esry, and I. Ben-Itzhak, Phys. Rev. Lett. **111**, 163004 (2013).

[23] A. S. Alnaser, M. Kübel, R. Siemering, B. Bergues, N. G. Kling, K. J. Betsch, Y. Deng, J. Schmidt, Z. A. Alahmed, A. M. Azzeer, J. Ullrich, I. Ben-Itzhak, R. Moshammer, U. Kleineberg, F. Krausz, R. de Vivie-Riedle, and M. F. Kling, Nat. Commun. **5**, 3800 (2014).

[24] S. Miura, T. Ando, K. Ootaka, A. Iwasaki, H. Xu, T. Okino, K. Yamanouchi, D. Hoff, T. Rathje, G. G. Paulus, M. Kitzler, A. Baltuška, G. Sansone, and M. Nisoli, Chem. Phys. Lett. **595–596**, 61 (2014).

[25] U. Lev, L. Graham, C. B. Madsen, I. Ben-Itzhak, B. D. Bruner, B. D. Esry, H. Frostig, O. Heber, A. Natan, V. S. Prabhudesai, D. Schwalm, Y. Silberberg, D. Strasser, I. D. Williams, and D. Zajfman, J. Phys. B **48**, 201001 (2015).

[26] M. Kübel, R. Siemering, C. Burger, N. G. Kling, H. Li, A. S. Alnaser, B. Bergues, S. Zherebtsov, A. M. Azzeer, I. Ben-Itzhak, R. Moshammer, R. de Vivie-Riedle, and M. F. Kling, Phys. Rev. Lett. **116**, 193001 (2016).

[27] T. Endo, H. Fujise, Y. Kawachi, A. Ishihara, A. Matsuda, M. Fushitani, H. Kono, and A. Hishikawa, Phys. Chem. Chem. Phys. **19**, 3550 (2017).

[28] D. Keefer and R. de Vivie-Riedle, Acc. Chem. Res. **51**, 2279 (2018).

[29] J. L. White, B. J. Pearson, and P. H. Bucksbaum, J. Phys. B **37**, L399 (2004).

[30] E. Wells, K. J. Betsch, C. W. S. Conover, M. J. DeWitt, D. Pinkham, and R. R. Jones, Phys. Rev. A **72**, 063406 (2005).

[31] A. T. J. B. Eppink and D. H. Parker, Rev. Sci. Instrum. **68**, 3477 (1997).

[32] R. Dörner, V. Mergel, O. Jagutzki, L. Spielberger, J. Ullrich, R. Moshammer, and H. Schmidt-Böcking, Phys. Rep. **330**, 95 (2000).

[33] J. Ullrich, R. Moshammer, A. Dorn, R. Dörner, L. P. H. Schmidt, and H. Schmidt-Böcking, Rep. Prog. Phys. **66**, 1463 (2003).

[34] B. J. Whitaker, *Imaging in Molecular Dynamics: Technology and Applications* (Cambridge University Press, Cambridge, UK, 2003).

[35] A. Zhao, M. van Beuzekom, B. Bouwens, D. Byelov, I. Chakaberia, C. Cheng, E. Maddox, A. Nomerotski, P. Svihra, J. Visser, V. Vrba, and T. Weinacht, Rev. Sci. Instrum. **88**, 113104 (2017).

[36] A. G. Suits, Rev. Sci. Instrum. **89**, 111101 (2018).

[37] A. S. Alnaser, T. Osipov, E. P. Benis, A. Wech, B. Shan, C. L. Cocke, X. M. Tong, and C. D. Lin, Phys. Rev. Lett. **91**, 163002 (2003).

[38] A. S. Alnaser, S. Voss, X. M. Tong, C. M. Maharjan, P. Ranitovic, B. Ulrich, T. Osipov, B. Shan, Z. Chang, and C. L. Cocke, Phys. Rev. Lett. **93**, 113003 (2004).

[39] N. G. Johnson, O. Herrwerth, A. Wirth, S. De, I. Ben-Itzhak, M. Lezius, B. Bergues, M. F. Kling, A. Senftleben, C. D. Schröter,

R. Moshammer, J. Ullrich, K. J. Betsch, R. R. Jones, A. M. Sayler, T. Rathje, K. Rühle, W. Müller, and G. G. Paulus, Phys. Rev. A **83**, 013412 (2011).

[40] P. Sándor, V. Tagliamonti, A. Zhao, T. Rozgonyi, M. Ruckenbauer, P. Marquetand, and T. Weinacht, Phys. Rev. Lett. **116**, 063002 (2016).

[41] W. Zhang, X. Gong, H. Li, P. Lu, F. Sun, Q. Ji, K. Lin, J. Ma, H. Li, J. Qiang, F. He, and J. Wu, Nat. Commun. **10**, 757 (2019).

[42] K. Sändig, H. Figger, and T. W. Hänsch, Phys. Rev. Lett. **85**, 4876 (2000).

[43] D. Pavičić, A. Kiess, T. W. Hänsch, and H. Figger, Phys. Rev. Lett. **94**, 163002 (2005).

[44] V. S. Prabhudesai, U. Lev, A. Natan, B. D. Bruner, A. Diner, O. Heber, D. Strasser, D. Schwalm, I. Ben-Itzhak, J. J. Hua, B. D. Esry, Y. Silberberg, and D. Zajfman, Phys. Rev. A **81**, 023401 (2010).

[45] X. Xie, S. Roither, M. Schöffler, E. Lötstedt, D. Kartashov, L. Zhang, G. G. Paulus, A. Iwasaki, A. Baltuška, K. Yamanouchi, and M. Kitzler, Phys. Rev. X **4**, 021005 (2014).

[46] A. M. Sayler, J. McKenna, B. Gaire, N. G. Kling, K. D. Carnes, B. D. Esry, and I. Ben-Itzhak, J. Phys. B: At., Mol. Opt. Phys. **47**, 031001 (2014).

[47] W. Cao, G. Laurent, I. Ben-Itzhak, and C. L. Cocke, Phys. Rev. Lett. **114**, 113001 (2015).

[48] A. Shahi, Y. Albeck, and D. Strasser, J. Phys. Chem. A **121**, 3037 (2017).

[49] A. Hishikawa, S. Liu, A. Iwasaki, and K. Yamanouchi, J. Chem. Phys. **114**, 9856 (2001).

[50] A. M. Sayler, P. Q. Wang, K. D. Carnes, B. D. Esry, and I. Ben-Itzhak, Phys. Rev. A **75**, 063420 (2007).

[51] M. Zohrabi, J. McKenna, B. Gaire, N. G. Johnson, K. D. Carnes, S. De, I. A. Bocharova, M. Magrakvelidze, D. Ray, I. V. Litvinyuk, C. L. Cocke, and I. Ben-Itzhak, Phys. Rev. A **83**, 053405 (2011).

[52] W. Cao, G. Laurent, S. De, M. Schöffler, T. Jahnke, A. S. Alnaser, I. A. Bocharova, C. Stuck, D. Ray, M. F. Kling, I. Ben-Itzhak, T. Weber, A. L. Landers, A. Belkacem, R. Dörner, A. E. Orel, T. N. Rescigno, and C. L. Cocke, Phys. Rev. A **84**, 053406 (2011).

[53] X. Gong, P. He, Q. Song, Q. Ji, K. Lin, W. Zhang, P. Lu, H. Pan, J. Ding, H. Zeng, F. He, and J. Wu, Optica **3**, 643 (2016).

[54] M. Kunitski, N. Eicke, P. Huber, J. Köhler, S. Zeller, J. Voigtsberger, N. Schlott, K. Henrichs, H. Sann, F. Trinter, L. P. H. Schmidt, A. Kalinin, M. S. Schöffler, T. Jahnke, M. Lein, and R. Dörner, Nat. Commun. **10**, 1 (2019).

[55] I. Ben-Itzhak, P. Q. Wang, J. F. Xia, A. M. Sayler, M. A. Smith, K. D. Carnes, and B. D. Esry, Phys. Rev. Lett. **95**, 073002 (2005).

[56] P. A. Orr, I. D. Williams, J. B. Greenwood, I. C. E. Turcu, W. A. Bryan, J. Pedregosa-Gutierrez, and C. W. Walter, Phys. Rev. Lett. **98**, 163001 (2007).

[57] H. Hultgren and I. Y. Kiyan, Phys. Rev. A **84**, 015401 (2011).

[58] D. M. Kandhasamy, Y. Albeck, K. Jagtap, and D. Strasser, J. Phys. Chem. A **119**, 8076 (2015).

[59] P. Wustelt, F. Oppermann, L. Yue, M. Möller, T. Stöhlker, M. Lein, S. Gräfe, G. G. Paulus, and A. M. Sayler, Phys. Rev. Lett. **121**, 073203 (2018).

[60] J. McKenna, A. M. Sayler, B. Gaire, N. G. Johnson, K. D. Carnes, B. D. Esry, and I. Ben-Itzhak, Phys. Rev. Lett. **103**, 103004 (2009).

[61] B. Jochim, B. Berry, T. Severt, P. Feizollah, M. Zohrabi, Kanaka Raju P., E. Wells, K. D. Carnes, and I. Ben-Itzhak, J. Phys. Chem. Lett. **10**, 2320 (2019).

[62] G. C. Goode and K. R. Jennings, *Advances in Mass Spectrometry*, edited by A. R. West (Applied Science Publishers, London, 1974), Vol. 6.

[63] K. M. Ervin, J. Ho, and W. C. Lineberger, J. Chem. Phys. **91**, 5974 (1989).

[64] M. J. Jensen, U. V. Pedersen, and L. H. Andersen, Phys. Rev. Lett. **84**, 1128 (2000).

[65] S. Hayakawa, M. Takahashi, K. Arakawa, and N. Morishita, J. Chem. Phys. **110**, 2745 (1999).

[66] J. McKenna, A. M. Sayler, F. Anis, N. G. Johnson, B. Gaire, U. Lev, M. A. Zohrabi, K. D. Carnes, B. D. Esry, and I. Ben-Itzhak, Phys. Rev. A **81**, 061401(R) (2010).

[67] B. Jochim, M. Zohrabi, T. Severt, B. Berry, K. J. Betsch, P. Feizollah, J. Rajput, E. Wells, K. D. Carnes, and I. Ben-Itzhak, Phys. Rev. A **101**, 013406 (2020).

[68] T. Severt, M. Zohrabi, K. J. Betsch, B. Jochim, B. Berry, T. Uhlíková, and B. D. Esry (in preparation).

[69] P. Q. Wang, A. M. Sayler, K. D. Carnes, J. F. Xia, M. A. Smith, B. D. Esry, and I. Ben-Itzhak, Phys. Rev. A **74**, 043411 (2006).

[70] A. M. Sayler, Measurements of ultrashort intense laser-induced fragmentation of simple molecular ions, Ph.D. thesis, Kansas State University, 2008.

[71] R. Trebino, K. W. DeLong, D. N. Fittinghoff, J. N. Sweetser, M. A. Krumbügel, B. A. Richman, and D. J. Kane, Rev. Sci. Instrum. **68**, 3277 (1997).

[72] The peak intensity of the pulse is evaluated by picking off a portion of the beam after the parabolic focusing mirror and imaging the laser beam profile with a CCD camera, as described in Ref. [73].

[73] A. M. Sayler, P. Q. Wang, K. D. Carnes, and I. Ben-Itzhak, J. Phys. B **40**, 4367 (2007).

[74] The laser beam waist is of the order of tens of μm, and the ion beam width is about 0.9 mm.

[75] R. W. Boyd, *Nonlinear Optics*, 3rd ed. (Academic Press, Orlando, FL, 2008).

[76] D. Edvardsson, M. Lundqvist, P. Baltzer, B. Wannberg, and S. Lunell, Chem. Phys. Lett. **256**, 341 (1996).

[77] R. Baková, J. Fišer, T. Šedivcová-Uhlíková, and V. Špirko, J. Chem. Phys. **128**, 144301 (2008).

[78] F. von Busch and G. H. Dunn, Phys. Rev. A **5**, 1726 (1972).

[79] H. Helm and P. C. Cosby, J. Chem. Phys. **86**, 6813 (1987).

[80] Z. Amitay, A. Baer, M. Dahan, J. Levin, Z. Vager, D. Zajfman, L. Knoll, M. Lange, D. Schwalm, R. Wester, A. Wolf, I. F. Schneider, and A. Suzor-Weiner, Phys. Rev. A **60**, 3769 (1999).

[81] E. Y. Sidky and I. Ben-Itzhak, Phys. Rev. A **60**, 3586 (1999).

[82] C. Cornaggia and P. Hering, Phys. Rev. A **62**, 023403 (2000).

[83] J. McKenna, F. Anis, A. M. Sayler, B. Gaire, N. G. Johnson, E. Parke, K. D. Carnes, B. D. Esry, and I. Ben-Itzhak, Phys. Rev. A **85**, 023405 (2012).

[84] J. McKenna, F. Anis, B. Gaire, N. G. Johnson, M. Zohrabi, K. D. Carnes, B. D. Esry, and I. Ben-Itzhak, Phys. Rev. Lett. **103**, 103006 (2009).

[85] A. M. Sayler, J. McKenna, B. Gaire, N. G. Kling, K. D. Carnes, and I. Ben-Itzhak, Phys. Rev. A **86**, 033425 (2012).

[86] P. Q. Wang, A. M. Sayler, K. D. Carnes, B. D. Esry, and I. Ben-Itzhak, Opt. Lett. **30**, 664 (2005).

[87] I. Ben-Itzhak, P. Q. Wang, A. M. Sayler, K. D. Carnes, M. Leonard, B. D. Esry, A. S. Alnaser, B. Ulrich, X. M. Tong, I. V. Litvinyuk, C. M. Maharjan, P. Ranitovic, T. Osipov, S. Ghimire, Z. Chang, and C. L. Cocke, Phys. Rev. A **78**, 063419 (2008).

[88] B. Jochim, R. Erdwien, Y. Malakar, T. Severt, B. Berry, P. Feizollah, J. Rajput, B. Kaderiya, W. L. Pearson, K. D. Carnes, A. Rudenko, and I. Ben-Itzhak, New J. Phys. **19**, 103006 (2017).

[89] The KER resolution in our experimental setup scales with $\sqrt{\text{KER}}$ [69]. We estimate the KER resolution in the present measurement by scaling from a previous measurement of dissociation of vibrationally cold CO^{2+} [66], wherein the instrumental broadening dominated. In our convolution, we used a Gaussian response function with a width evaluated at the peak centroid, thus neglecting the small variation of the resolution across the narrow peaks.

[90] A. Talebpour, S. Larochelle, and S. L. Chin, J. Phys. B **30**, 1927 (1997).

[91] C. Guo and K. Wright, Phys. Rev. A **71**, 021404(R) (2005).

[92] C. Guo, J. Phys. B **38**, L323 (2005).

[93] J. Wu, H. Zeng, and C. Guo, J. Phys. B **39**, 3849 (2006).